Hindawi
Journal of Nanomaterials
Volume 2023, Article ID 3456536, 15 pages
https://doi.org/10.1155/2023/3456536

Research Article

An Analysis of the Effects of Nanofluid-Based Serpentine Tube Cooling Enhancement in Solar Photovoltaic Cells for Green Cities

J. Prakash Arul Jose,[1] Anurag Shrivastava,[2] Prem Kumar Soni,[3] N. Hemalatha,[4] Saad Alshahrani,[5] C. Ahamed Saleel,[5] Abhishek Sharma,[6] Saboor Shaik,[7] and Ibrahim M. Alarifi[8]

[1]*Paavai Engineering College, Namakkal, India*
[2]*Saveetha School of Engineering, Saveetha Institute of Medical and Technical Sciences, Chennai, Tamilnadu, India*
[3]*Department of Mechanical Engineering, Lakshmi Narain College of Technology and Science, Bhopal, India*
[4]*Institute of Electronics and Communication Engineering, Saveetha School of Engineering (SIMATS), Chennai, India*
[5]*Department of Mechanical Engineering, College of Engineering, King Khalid University, PO Box 394, Abha 61421, Saudi Arabia*
[6]*Department of Mechanical Engineering, Birsa Institute of Technology Sindri, Dhanbad 828123, Jharkhand, India*
[7]*School of Mechanical Engineering, Vellore Institute of Technology, Vellore 632014, Tamil Nadu, India*
[8]*Department of Mechanical and Industrial Engineering, College of Engineering, Majmaah University, Al-Majmaah 11952, Riyadh, Saudi Arabia*

Correspondence should be addressed to Anurag Shrivastava; anuragshri76@gmail.com, Abhishek Sharma; drasharma58@gmail.com and Ibrahim M. Alarifi; i.alarifi@mu.edu.sa

Received 4 July 2022; Accepted 25 November 2022; Published 20 January 2023

Academic Editor: Mohammad Rahimi-Gorji

In this work, the impact of the serpentine copper tube heat exchanger with nanofluids on 100 W solar photovoltaic thermal collectors (PV/T) was analyzed experimentally and numerically. The cooling fluids assessed in this system were distilled water, Al_2O_3 0.1%, and Al_2O_3 0.2% based nanofluids. Tests were accomplished at diverse coolant mass flow rate in India's summer days of 2018. A computational fluid dynamics (CFD) investigation was carried out to perform a parametric study, identify surface and exit T profiles, and examine the cooling effectiveness. The impact of mass flow rate of nanofluid on the outside T and Reynolds number were studied. The Reynolds number obtained in the flow experiments and CFD analysis was in the range of 900–1,300. The maximum irreversibility occurred while using water, whereas minimum irreversibility obtained Al_2O_3 0.2% nanofluid. Exergy efficiency was found to be increased from 20% to 36% during the day. It was identified that the increase in PV/T scheme led to higher exergy losses. The thermal efficiency of a water-based cooling system resulted in 53.61%. Meanwhile, Al_2O_3 0.1% and Al_2O_3 0.2% based coolants provided 69.45% and 71.02%, respectively. A good agreement was obtained between the experimental results and the computer model.

1. Introduction

Nowadays, more existing cities are getting converted into green and smart cities. There are tremendous benefits in greening existing cities. Green and smart cities are mutually inclusive and would offer tangible and intangible benefits. It is learned that the greening of existing cities achieves an 11%–13% decrease in power demand due to a higher share of solar thermal, photovoltaic, and other renewable energy.

A solar PV/T converts solar emissions to electrical energy and thermal energy simultaneously. It is a series of solar cell that changes solar rays into electricity and a solar heat collector that absorbs the rest energy and keeps away left-over heat from a PV study. Due to this setup, the overall energy effectiveness of PV/T is more than that of solar photovoltaic (PV) or separate solar thermal collectors. A rise in T occurred due to heat production, reducing the efficacy of solar cells while operating. Consequently, a heat-carrying mechanism is needed from the PV cells to offer the cooling effect to cells and lower the resistance, which leads to an increase in efficiency [1]. An solar photovoltaic/thermal (SPV/T) collector is basically a conductive metal structure

in a hollow shape for placing the PV panels. Heat is radiated from these panels into a covered hole of the shallow metal box. The T where a PV module operates is equivalent to the total of the heat it generates and the heat it loses to the surroundings. The PV module's T and the other materials it came into touch with differed, which led to conductive energy loss. The thermal conductivity of a PV module determines its option to transmit heat to its environment. The transmission of heat away from a surface. Consequently, one substance moving from across the top of another is called convective heat transfer (CHT). CHT occurs in PV modules when the wind blows around the module's surface. Radiation is the final method whereby the PV module can transport T of the surrounding atmosphere.

Dwivedi et al. [1], Shahsavar et al. [2], and Hossain et al. [3] proved that heat removal from a solar PV system is effective while using water or nanofluids as a cooling medium. Lalović et al. [4] and Alzaabi et al. [5] proposed a design of collector pipes to upsurge the contact arena among the pipes and PV panels to increase the heat transfer (HT). Yu et al. [6] and Azari et al. [7] have examined the laminar-forced convection flows through water–Al_2O_3 nanofluids. They showed that increasing the Al_2O_3 volume fraction could improve the heat transfer rate. Gupta and Prasad [8] and Ranga Babu et al. [9] performed a comprehensive study with Al_2O_3, SiO_2, CuO, and vegetable oil–water emulsion to examine HT capabilities.

Bellos et al. [10] and Rasheed et al. [11] concluded that the HT coefficient enhanced considerably with the increased nanoparticle concentration. Qeays et al. [12], Bambrook et al. [13], and Leong et al. [14] found that the friction factor increased with the use of nanofluids though there is an increase in HT rate. Wole-Osho et al. [15] investigated the effects of ZnO–water (0.5%) nanofluids on the HT of flat plate collectors (FPC). The result displayed that a higher T gradient could be achieved than that of water. Ajay and Kundan [16] evaluated the applications of SiO_2 and CuO of 20 nm nanofluids of 0.01% volume concentration in a parabolic-shaped concentrating solar collector. They demonstrated that the efficiency of collector is improved by 6% while using SiO_2 and CuO.

Moghadam et al. [17], Ekramian et al. [18], and Shafiey et al. [19] analyzed CuO–water-based nanofluid impact on a solar collector in comparison to water. The outcomes showed that an increase in the mass fraction of nanofluid decreases the specific heat. In turn, less energy was needed to raise the T. Mahian et al. [20] investigated the HT features of Al_2O_3/water nanofluid with a particle size of 25, 50, 75, and 100 nm, with volume concentrations up to 4% and at a constant discharge in a solar collector. The HT coefficient values and Nusselt number were considerably affected by the uncertainties in thermophysical models and tube roughness. An energy life cycle assessment of nanofluid-based PV/T, PV, and traditional PV/T systems was carried out by Hossain et al. [21]. In comparison to PV and PV/T systems, it was found that the yearly exergy output of 1.3 MWh/m^2 had the lowest exergy payback of 2 years for nanofluid-based PV/T. Highest heat efficiency of 70% with active solar still was reached by Singh et al. [22] after doing an experimental and theoretical analysis on PV/T system coupled solar still. The performance and stability improvement of the SiC nanofluid in the ST collector was examined by Li et al. [23]. For a 1 wt% SiC nanofluid, they observed a peak solar conversion efficiency of 96.8%. Verma et al. [24] conducted an experimental assessment of the effect of several nanofluids on the enhancement of ST collector power. It was found that the Mg nanofluids exhibit more power production than the CuO nanofluids. Numerical analysis was performed by Wole-Osho et al. [25] to determine how Al_2O_3 water nanofluid affected the PVT system's performance. A peak thermal energy performance of 89% was found. Salari et al. [26] tested a PVT module with phase change material in their numerical study. They chose a variety of nanofluids, such as MWCNT, MgO, and MgO/MWCNT hybrid nanofluids. The PVT module with a hybrid nanofluid demonstrated an overall power performance of 58.66%. Ma et al. [27] developed a 2D numerical model to calculate the effects of numerous variables on the power output of the PVT–ST system, including flow rate, irradiation, and coolant inflow temperature. The PVT–ST system's annual electrical and thermal power outputs were found to be 298.5 and 2,096.5 kWh, respectively. Additionally, utilizing a 2D mathematical model, a numerical study on the PVT–ST water-based system was carried out in another study [28]. According to the findings, the combined system that has glass covers on both the PVT and ST components exhibits the best overall power and energy performance. An innovative hybrid drying equipment which is powered by a solar PV/T air collector and a wind turbine was designed and tested to address the issue of a solar drying device's inadequate energy supply by Kong et al. [29]. The findings showed that the energy generated by solar and wind energy satisfied the needs of the drying system for continuous operation. On the effectiveness of PV/T, the impact of nanofluid stability and synthesizing techniques was assessed by Parsa et al. [30]. The impact of flow patterns in various nanofluid types on the PV/T system was also investigated. It was observed that compared to the two-step preparation process, the energy and exergy of the PV/T for one-step nanofluid were significantly enhanced. Additionally, it was found that by increasing nanofluid in a one-step approach from 1%–3% to 3%–5%, all efficiencies rose linearly. In order to determine the least entropy generation dependent on the second law of TD, Chauhan et al. [31] devised a simple solar PV/T model. They found that the minimum entropy generation of PVT systems is in the range of 500–526 W and the peak temperature difference could reach 18°C, resulting in a 9.6% improvement in electrical efficiency. A numerical model developed by Ooshaksaraei et al. [32] was used to assess the energy and exergy efficiency of the PV/T system. It was found that when the packing factor was 0.7, the exergy efficiency could reach 9.5%, and when the flow rate varied was increased, the system's energy efficiency also increased. In order to look into system irreversibility, Rashidi et al. [33] reviewed the entropy production of numerous solar thermal energy systems. According to their analysis, they found that the entropy generation reduction method of designing is the best option for solar energy systems.

In a glazed tube and sheet PV/T system with a heat exchanger, Jakhar et al. [34] evaluated the performance of an alumina/water nanofluid in a semiarid location in Pilani, Rajasthan (India). Under equal Re comparison, they found

that the PV/T system with NF performs better. Improvements include a 2°C drop in PV panel temperature, a 6°C drop in the temperature difference between the PV/T outlet and input, a 0.1% increase in electrical efficiency, and a 4% increase in thermal efficiency. In a similar study, Jakhar et al. [35] assessed the effectiveness of the PV/T system using various nanoparticles. They found that with nanoparticles, the HTC rises and varies between 250.6 and 529.20 W/m^2 K, 255.42 and 539.8 W/m^2 K, and 261.1 and 550.8 W/m^2 K for volume fractions of 0.5%, 1.0%, and 1.5%, respectively, for Reynolds numbers of 250–1,500. Jakhar et al. [36] also proposed an earth water heat exchanger (EWHE), a unique PV panel cooling system, and modeled using TRNSYS v17.0 software for the conditions in Pilani, Rajasthan (India). They found that the PV panel's temperature decreases to 46.29°C when connected to a EWHE system and their efficiency increases to 11% with a mass flow rate of 0.022 kg/s. A PVT system was evaluated by Yazdanifard et al. [37] for laminar and turbulent flows using nanofluids. They concluded that the presence of nanoparticles improved overall performance. Al_2O_3/water, TiO_2/water, and ZnO/water are three different forms of nanofluids that were used in the numerical analysis of the sheet- and tube-type PVT system by Sardarabadi and Passandideh-Fard [38]. They found that in terms of electrical performance, the TiO_2/water- and ZnO/water-based PVT systems outperform the Al_2O_3/water-based PVT system. Moradgholi et al. [39] employed a combination of methanol and Al_2O_3 to carry out an experimental inquiry to evaluate the impact of a nanofluid. According to their findings, the addition of the nanofluid increases power generation by 1.4 (W) as a result of a 14.5 (°C) drop in temperature. Purohit et al. [40] carried out yet another numerical analysis to assess the effects of nanofluid on the PVT system in laminar flow. For different nanoparticle concentrations and Reynolds numbers, they looked at two scenarios of pure water and the water/alumina nanofluid in the PVT. It was reported that, when nanoparticles are added, the HT coefficient rises by 25.2% as compared to pure fluid at fixed Reynolds numbers. Jidhesh et al. [41] carried out thermal modeling for a semitransparent photovoltaic–thermal hybrid collector using CuO nanofluid. They found that the overall exergy efficiency of SPV–THC employing CuO nanofluid and water rose by 26% and 12.25%, respectively, when compared to a standard PV system. Shahsavar et al. [42] carried out an experimental investigation to find the energy and exergy performance of a nanofluid-based photovoltaic thermal unit outfitted with a grooved helical microchannel heat sink. It was seen that the staggered unit has an overall energy efficiency of 17.05%, which is 6.96% greater than the simple and parallel units. In another study, Shahsavar et al. [43] conducted an experimental examination into the impacts of a water/magnetite nanofluid and flow channel configuration on PVT systems. It was found that the PVT-8S system offers the most effective configuration since its total energy efficiency is 5% : 87% greater than that of the PVT-4S system and 15% : 59% higher than that of the PVT-0S system.

It has been identified from the above literature study that the effect of using a sinusoidal serpentine tube on the overall performances of a nanofluid-based PVT system has not been attempted experimentally. Even though researchers have achieved substantial advancements in cooling for SPV/T systems, exergy losses are still being reported at a high level. To boost the rate of HT, liquid cooling improvement devices must fundamentally have an optimum design. However, there are not many documents in the literary works on liquid cooling systems that use purified water, Al_2O_3 0.1%, and Al_2O_3 0.2% in the serpentine tube heat exchangers to lower the T rise of PV/T systems. This study intends to examine the arrangement of serpentine tube heat exchangers with nanofluids to fill this research gap. This serpentine tube holds a huge HT region in a little space with a higher coefficient of HT. The coolant arrives at the bottom side of the heat exchanger and carries away the Tedlar heat engrossed at the bottommost of the solar PV board. The solar flux and flow have always been uniformly distributed in most numerical simulations using 1D or 2D analysis, and many relationships in the models are similarly predicated on a uniform T. The stream will be heated unevenly and, thus, will be nonuniform due to the nonuniform solar flux upon on outermost layer of the inner absorber tube.

This experimental and computational study aims to (1) conduct an energy study for a 100 W solar PV/T collector by a serpentine tube heat exchanger using the first and second laws of effectiveness. (2) Conduct computational fluid dynamics (CFD) investigation to perform a parametric study and identify surface and exit T profiles, for three liquids at different mass flow rates to analyze the cooling effectiveness.

2. Experimental Strategy

2.1. Test Setup. This experimental system comprises a 100 W SPV/T of capacity with a collector area of 0.915 m^2. A serpentine tube heat exchanger was fitted under the solar panel absorber plate. The working fluids considered were pure water and aluminium oxide (Al_2O_3) with nanoparticles varied in water concentration (φ) 0.1% and 0.2% (w/v), which is used as base fluid (BF). They were supplied over the serpentine flow copper tube heat exchanger by the mass flow rate of 0.015, 0.0133, and 0.0117 kg/s. These values were chosen based on the similar kind of experiments available in the surveyed literature.

Anna University in Chennai designed, created, and verified the test setup. In Chennai (13° 06 North, 80° 18 East), readings were taken from April to June 2018. On all days of the testing, values were measured between 9 am and 5 pm. The first law of efficiency was used for energy assessment, whereas the second law of efficiency was used for exergy studies to determine energy losses in a PV conversion operation.

The test setup and its schematic figure are shown in Figures 1(a) and 1(b). This PV/T system mainly consists of components like, (1) PV thermal unit, (2) serpentine copper tube heat exchanger arrangement, (3) collection tanks, (4) datalogger, and (5) other accessories, such as flow meter, boosting pump, valves, and thermocouples. The SPV/T system was supported by a frame made of galvanized metal, allowing solar energy to quickly pass over a glass surface. In order to avoid rain and other natural occurrences, it was positioned 120 mm above the ground. It was made sure that the system

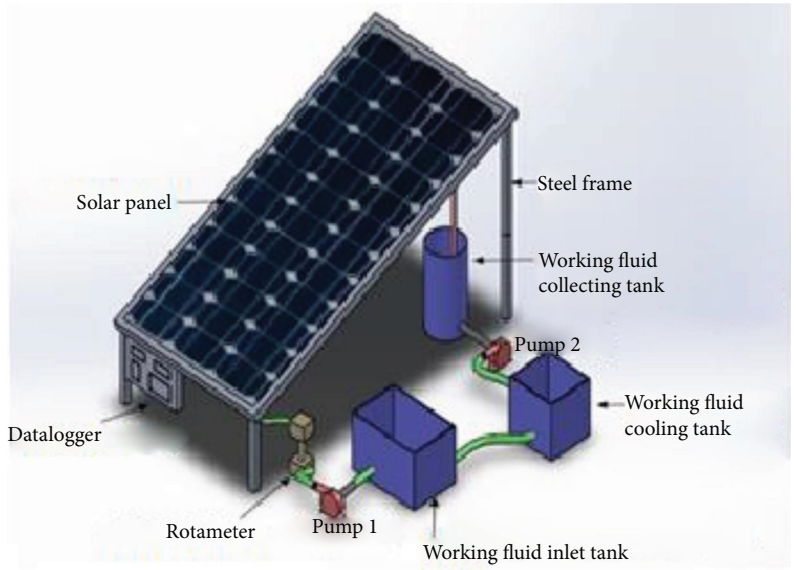

(a)

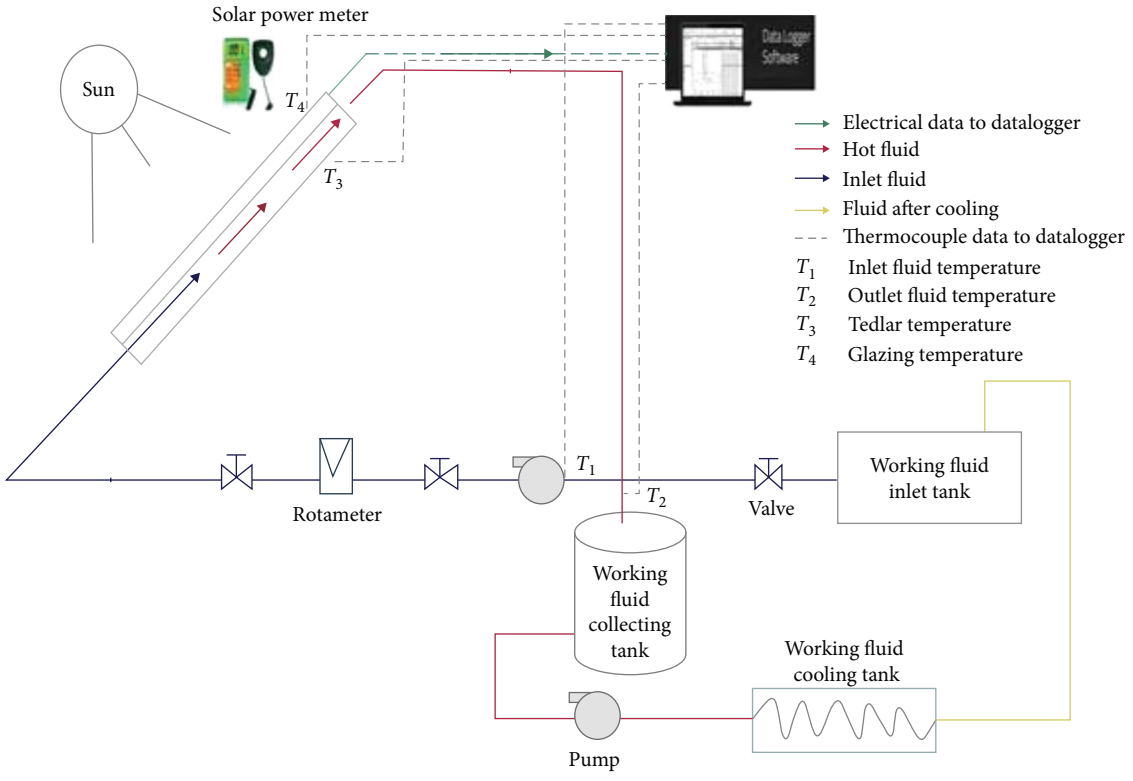

(b)

Figure 1: (a) SPV/T test setup; (b) SPV/T test setup schematic illustration.

was shadow-free; and as per the Chennai meteorological website, the SPV/T system's angle has been set at 13°. The SPV/T scheme and operating constraints are specified in Tables 1–3.

A booster pump was employed to supply the coolant through a controlling valve. A thermocouple was introduced to the pipe connections to measure the inlet T. A flow meter was fitted to quantify the coolant flow rate. The thermocouples positioned along with below the solar PV panel measured the glazing and Tedlar (T_s). Across the trial period, a datalogger recorded all T values in short (10 s) steps. Using a pyranometer, experimental results of sun radiation were gathered and processed at a normal time interval of 30 min.

2.2. Nanofluid Preparation. The 20 nm-sized Al_2O_3 nanoparticles with the purity of 99% and surface area of 40 m^2/g were used for this study. Two samples of nanofluids were prepared

Table 1: Specifications of solar PV/thermal scheme.

Tilt angle of solar panel	13°
Length of the PV module (L_1)	1,349 mm
Width of the PV module (L_2)	678 mm
PV module	0.915 mm^2
Length of the copper tube	510 mm
Diameter of the copper tube	15.95 mm
Short-circuit current of solar panel (ISC)	9.42 A
Load voltage (V_L)	17.50 V
Load current (A_L)	8.57 A
Number of cells	36
Slope of the solar panel surface	13
Overall loss coefficient (UL)	5 W/m^2 K
Transmittance of the glass cover (τ)	0.95
Absorptance of the glass cover (α)	0.85
Collector breadth (B)	658 mm
Collector breadth (H)	840 mm
Area of the panel (A)	98,042 mm^2
Air duct length (I)	1,470 mm
Air duct breadth (b)	645 mm
Air duct width (w)	80 mm
Cross section of air entry ($l \times b$)	149 × 80 mm

Table 2: Operating parameters.

Parameters	Measurement
Ambient temperature (T_a)	302–306 K
Solar radiation	700–1,200 W/m^2

by dispersing Al_2O_3 atoms with diverse φ of 0.1% and 0.2% (w/v) through water suspension.

$$\text{w/v}(\%) = \frac{\text{Mass of solute (g)}}{\text{Volume of solution (ml)}} \times 100. \quad (1)$$

Nanofluid thermophysical properties are listed in Table 2.

2.3. Uncertainty Analysis. All the instruments were calibrated before taking experimental readings to avoid uncertainties. The PV/T setup consisted of a voltmeter, T sensor, pyranometer, and pressure gauges. A mercury thermometer restrained ambient air T. Intake, exit air T, and glazing surface T be restrained by thermocouples and are placed at a proper position of the PV/T scheme. The flow of air was attuned through a valve placed between the blower and air channel intake. The sun's rays were restrained through a pyranometer that is situated identically to the collector surface.

Supplied air and wind velocities were restrained through Lutron AM-4206M digital anemometer and a cup anemometer, respectively. Current and voltage were restrained through a standardized ammeter and voltmeter of the datalogger. Each dataset was recorded in the frequency of 15 min intervals and to a datalogger. The uncertainties that occurred during the measurement are enlisted in Table 4.

Table 3: Water and nanofluid properties.

Parameters	ρ (kg/m^3)	C_p (J/kg K)	K (W/mk)
Water	1,000	4,182	0.6
Al_2O_3	3,960	773	30

Table 4: The uncertainties of measurements.

Equipment	Measurement	Uncertainty
Thermocouples	Inlet and outlet air channel temperature	±1°C
Thermocouples	Glazing and Tedlar temperatures	±1°C
Anemometer	Air velocity	±5%
Pyranometer	Solar radiation	±5%
Weather station	Wind velocity	±0.5 m/s
Mercury thermometer	Ambient temp	±0.5°C
PV short-circuit current	Current	±1%
PV open-circuit voltage	Voltage	±1%
Digital manometer	Pressure	±1%

3. Analysis Methodology

3.1. PV/T System Exergy Analysis. Exergy depends on the second law of efficiency. It is a metric for gauging system sustainability. It demonstrates how well the HT process works. Energy quality was included in the analysis for evaluating the most effective energy utilization. Assuming that the system is in a quasi-steady state, an increase in T maintains the air's constant specific heat.

The mass balance equation is expressed as follows:

$$\sum \dot{m}_{in} = \sum \dot{m}_{out}, \quad (2)$$

where $\dot{m}$ stands for flow rate, in denotes an intake, and out denotes an exit. The generalized energy and exergy balances can be expressed in rate form (after ignoring the effects of kinetic and potential energy fluctuations) [44]:

$$\sum \dot{E}_{in} = \sum \dot{E}_{out}, \quad (3)$$

$$\sum \dot{E}x_{in} - \sum \dot{E}x_{out} = \sum \dot{E}x_{irre}. \quad (4)$$

The rate form of the general exergy balance, using Equation (8), is as follows:

$$\sum \left(1 - \frac{T_a}{T_s}\right) \dot{Q}_s - \dot{W} + \sum \dot{m}_{in} \psi_{in} - \sum \dot{m}_{out} \psi_{out} = \dot{E}x_{irre}, \quad (5)$$

where

$$\psi_i = (h_{in} - h_a) - T_a(S_{in} - S_a), \quad (6)$$

$$\psi_o = (h_{out} - h_a) - T_a(S_{out} - S_a), \tag{7}$$

$$\left(1 - \frac{T_a}{T_s}\right)\dot{Q}_s - \dot{m}((h_{out} - h_{in}) - T_a(S_{out} - S_{in})) = \dot{E}x_{irre}, \tag{8}$$

where $\dot{Q}_s$ is the solar radiation absorbed by the panel's outside absorber.

$$\dot{Q}_s = G(\tau\alpha)A_{mod}. \tag{9}$$

The irreversibility is expressed as follows:

$$\dot{E}x_{iire} = T_a\,\dot{S}_{gen}, \tag{10}$$

$$\dot{S}_{gen} = \dot{m}C_p \ln\frac{T_o}{T_i} - \frac{\dot{Q}_s}{T_s} + \frac{Q_0}{T_a}, \tag{11}$$

$$Q_0 = \dot{Q}_s - \dot{m}C_p(T_o - T_i), \tag{12}$$

$$\eta_{\dot{E}x} = 1 - \frac{T_a\,\dot{S}_{gen}}{\left(1 - \frac{T_a}{T_s}\right)\dot{Q}_s}. \tag{13}$$

The net output exergy of a system or the exergetic devastation in the system is used to estimate the system's exergy effectiveness. The effectiveness of the second law is computed as follows:

$$\eta_{\dot{E}x} = \frac{\dot{E}x_o}{\dot{E}x_i} = \frac{\dot{m}(h_o - h_i - T_a(S_o - S_i))}{\left(1 - \frac{T_a}{T_s}\right)\dot{Q}_s}. \tag{14}$$

When using the exergy of a material contributor, it is important to note the distinction between exergy destruction and degradation [35–39]. Exergy losses include exergy that flows into the environment, whereas exergetic devastation denotes the irreversible lack of exergy inside the unit boundaries.

$$\dot{E}x_D = \frac{\dot{E}x_{irre}}{\dot{Q}_c.} \tag{15}$$

3.2. PV/T System Energy Analysis. The electrical efficacy of a PV study may be given as follows:

$$\eta_{el} = \frac{V_{mp}I_{mp}}{\dot{S}} = \frac{\dot{E}_{el}}{\dot{S}}. \tag{16}$$

Air mass flow rate is,

$$\rho = \frac{P}{RT_a}, \tag{17}$$

$$\dot{m} = \rho A_{mod}\nu. \tag{18}$$

The thermal efficacy of a PV/T is given as follows:

$$\dot{Q} = \dot{m}\,C_p(T_o - T_i), \tag{19}$$

$$\eta_{th} = \frac{\dot{m}\,C_p(T_o - T_i)}{A_{mod}G}. \tag{20}$$

The bulk average T is used to indicate all of the physical properties of the liquid.

$$\Delta T_m = \frac{T_i + T_o}{2}. \tag{21}$$

The total HT coefficient "h" for the unit may be considered as the liquid coolants acquired heat within the computed control volume. Therefore, the Nusselt number may be determined from Equation (22):

$$\mathrm{Nu} = h \cdot \frac{D}{k_{fluid}}. \tag{22}$$

Pressure drop of the system,

$$\Delta p = \left(f.\left(\frac{L}{D}\right)\rho U_m^2/2\right), \tag{23}$$

where ρ is the density of coolant and U_m is the coolant mean velocity.

3.3. Data Reduction. The mean air $T_f : T_f = T_{ai} + T_{ao}/2$ is restrained arithmetic mean coolant values of T at the system inlet and outlet.

The average plate T is calculated from plate thermocouples.

$$T_p = \frac{\sum_{i=1}^{n} T_{pi}}{n}, \tag{24}$$

where n is the number of thermocouples on the absorber plate. The mean flow area is used to compute the air velocity leaving the duct [40–45].

$$V = \frac{\dot{m}}{\rho}WH. \tag{25}$$

The rectangular duct section's hydraulic diameter is shown in Equation (26):

$$D_h = \frac{4\ (W \cdot H)}{2\ (W + H)}. \tag{26}$$

Therefore, the Nusselt number may be determined from Equation (27):

$$\mathrm{Nu} = \frac{hD_h}{k}. \tag{27}$$

4. CFD Analysis

It is a simulation technique used to solve complex fluid mechanics, and other related branches problems. Creation of a 2D or 3D model is the first step in CFD. A system of partial differential equations that specify the airflow was used to create the CFD model of the PV/T system.

4.1. Governing Equations (28)–(30). The following equations were used in this method to predict the flow features.

(1) The continuity equation:

$$\frac{\partial \rho}{\partial t} + \nabla \cdot \left(\rho \overrightarrow{V}\right) = 0. \tag{28}$$

(2) Navier–Stokes equation:

$$\frac{\partial u_i \rho}{\partial t} + \frac{\partial \left(u_i u_j\right)}{\partial x_j} = -\frac{1}{\rho}\frac{\partial p}{\partial x_i} + \frac{\partial}{\partial x_j}\left(\nu \frac{\partial u_i}{\partial x_j}\right). \tag{29}$$

(3) HT equations:

$$\frac{\partial T}{\partial t} + \frac{\partial}{\partial x_j}\left(u_j T\right) = \frac{\partial}{\partial x_j}\left(\alpha \frac{\partial T}{\partial x_j}\right). \tag{30}$$

In this study, Newtonian, incompressible, 3D, and transient assumptions were used for each of the three HT mechanisms. CFD code Ansys Fluent was used to solve the equations [46, 47]. Keeping in view of representing the physical model of the system presented above into a mathematical model, the following additional approximations and assumptions are made: (1) the flow is steady, laminar, incompressible, and 2D, (2) the coolant is Newtonian and viscous, (3) the thermophysical properties of the coolant are constant, and (4) the temperature gradient normal to the x–y planes is negligibly small.

4.2. Methodology of CFD Analysis. The flow field domain's continuum space was partitioned into suitably small discrete cells, whose distribution defines where the flow variables are computed and recorded. The mesh was hexahedral in shape and had an overall performance of 0.94, which would be acceptable for mesh processing in a CFD solver [48, 49]. An Octree is a spatial partition algorithm that discretizes the flow area into finite element analysis and is an object-oriented structural meshing method for discretizing the mathematical model. In addition, the Delaunay algorithm is employed to generate a smoother transition between some of the sizes of the control volumes. In Table 5, the mesh quality requirements used in CFD models are provided [50, 51].

Table 5: Grid quality requirements.

Factor	Quality criteria
Cell angle	>18°
Cell expansion rate	<10
Cell skewness	0.8–0.95
Aspect ratio	<1,000 for double precision solver
Orthogonal quality	>0.65

Table 6: Grid independence test.

Size of elements (mm)	Number of elements	Nusselt number (Nu)	Percentage difference
0.36	1,354,678	43.14	0.48
0.34	1,726,343	43.25	0.25
0.32	1,987,654	43.32	0.16

In Table 6, mesh-independence analysis was used to optimize the mesh size. The mesh size was adjusted when further meshing did not affect the simulated data [52–56]. Two million cells were chosen because there was no additional enhancement in the solution after such count, based on consistent with the experimental information.

The input information provided for computational analysis is cooling fluid properties such as density and viscosity and boundary conditions such as mass flow rate applied inside and outside the PV/T system. In addition, the K-epsilon (K-ε) turbulence model was selected as it is the validated and proven model for handling fluid turbulence. The pressure–velocity connection was performed by using the SIMPLE algorithm [57–61].

5. Results and Discussion

Energy and exergy tests were accomplished physically using the first and second law of efficacy, respectively, to investigate the effects of liquid cooling augmentation on solar system reversibility. The constructed numerical model was then used to verify the outputs.

5.1. Time Range of Experiment. Figure 2 shows the difference between solar radiation and the mean ambiance T over the test's 9–16 hr day experiment. Throughout the test's days, the ambient T ranged from 32 to 42°C, and the amount of solar radiation measured ranged between 600 and 1,100 W/m^2.

5.2. Influence of Liquid Cooling Enhancement on Exergy Performance. By taking into account the exergetic of solar radiation, the second law of efficiency was used to determine the exergy efficacy of a PV/T scheme with a serpentine heat exchanger. The energy destruction components were considered to determine irreversible losses affecting the SPV/T system. In addition, the exergy losses that occurred during the absorbing process were measured.

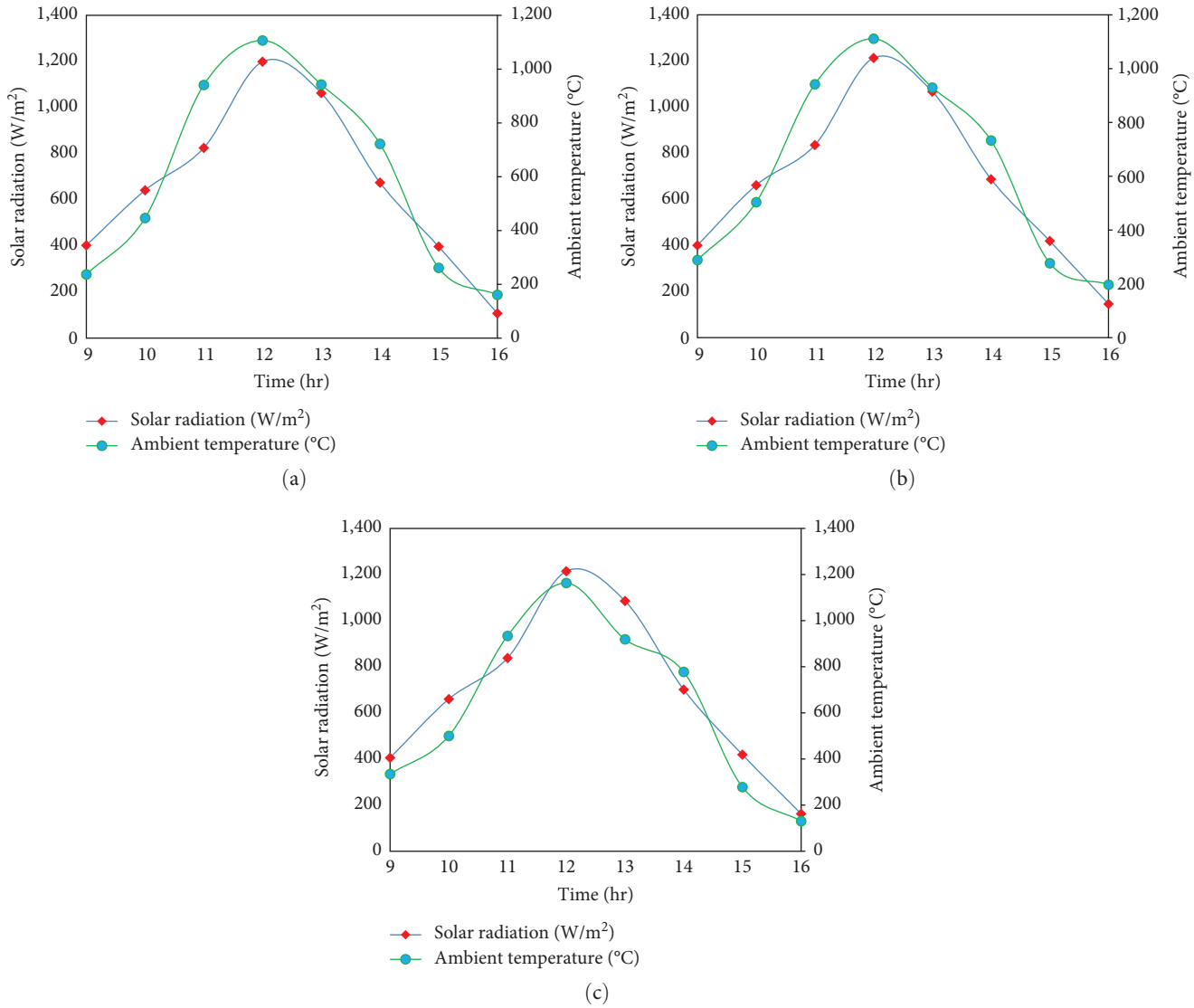

FIGURE 2: Solar radiation vs. air temperature at various mass flow rates. (a) $\dot{m}_1 = 0.015$ kg/s, (b) $\dot{m}_2 = 0.0133$ kg/s, and (c) $\dot{m}_3 = 0.0133$ kg/s.

The Al_2O_3 nanofluid with 0.2% concentration provided the maximum exergy efficiency of 36% while using a 0.015 kg/s mass flow rate (Figure 3(a)) as compared to $\dot{m} = 0.0133$ kg/s (Figure 3(b)) and $\dot{m} = 0.0117$ kg/s (Figure 3(c)). The energy efficiency was decreased to 30% at lesser mass flow rate of 0.0117 kg/s, as shown in Figures 4(b) and 4(c) [45]. The degree to which the SPV/T system's energy conversion process is irreversible determines the efficiency maintained. The material of PV modules in the solar panel also contributed to the loss of exergy. It was detected that the exergy efficacy increased when the solar intensity increased.

The maximum exergy efficacy recorded was 36% during the experiments. It was found that the variability of efficiency depends on the SPV/T system's energy conversion process' irreversibility [45]. This SPV/T system module has a 20% energy efficiency with no additional cooling. Due to its inability to capture all of the sun's energy, its efficiency was extremely poor. However, the tested serpentine tube heat exchanger with nanofluids raised the efficiency by 10%–16%, depending on the ambient conditions. When the sun's intensity rose, the energy efficiency rose as well. The exergy harm prevailed from 65% to 70%. The exergy destruction factor observed was 67%–72% with these cooling enhancements as compared to 88% of the bare SPV/T system.

5.3. Effect of Liquid Cooling Enhancement on Thermal Energy Efficiency. Numerous constraints like mass flow rate, specific heat, T drop, solar radiation, and nanofluid concentration contributed to the system's thermal efficiency. The heat cohort and elimination took place in diverse positions of the SPV/T system. In the absorber, the working fluid's thermal steadiness is strong-minded with regard to the amount of the heat energy pending out of the collector along with the energy mounted up through the employed liquid networks is equivalent to the relocated PV absorber energy towards waging fluid. The consolidated thermal efficacy of the SPV/T

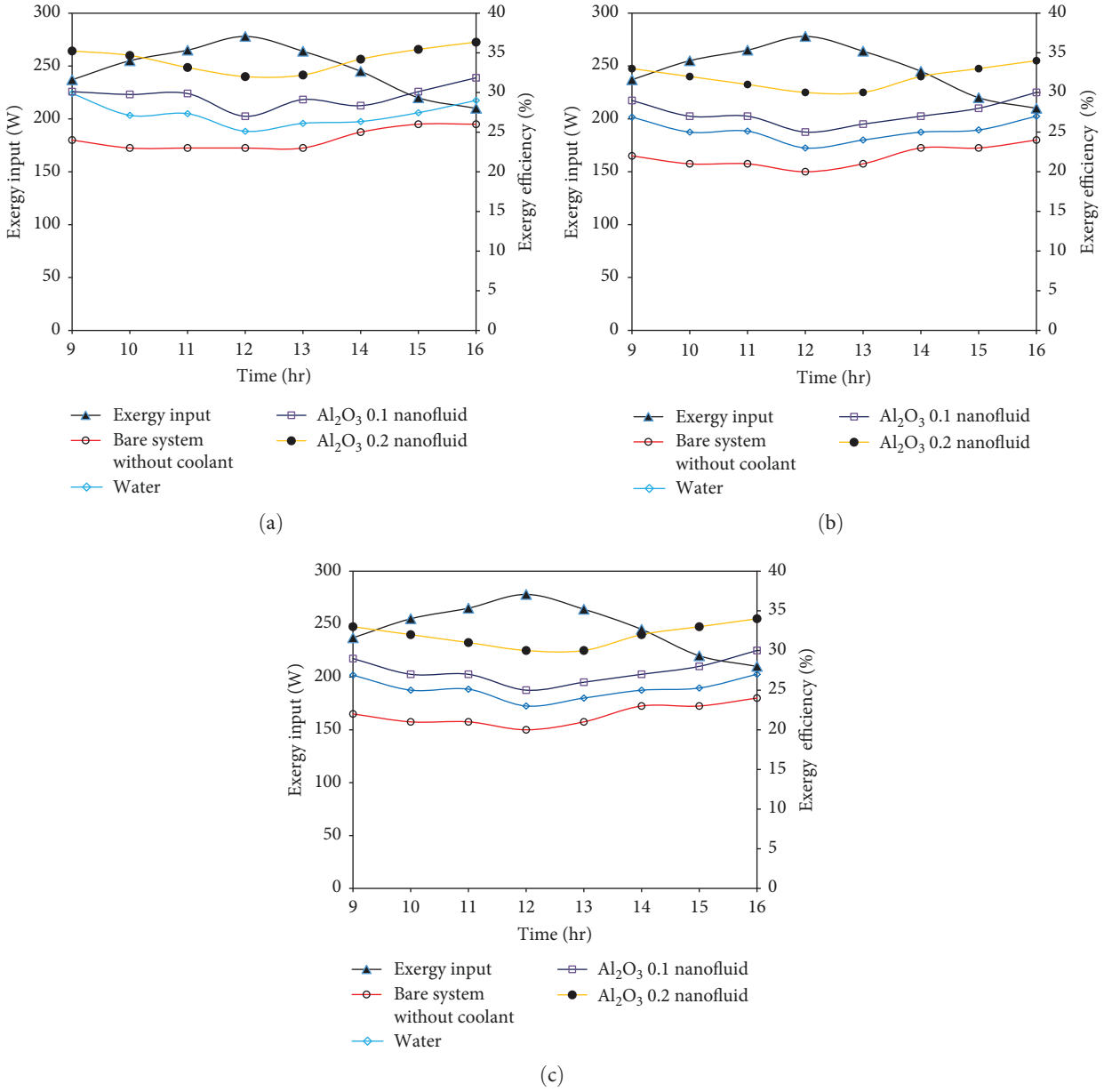

Figure 3: Exergy efficiency obtained at different mass flow rates. (a) $\dot{m} = 0.015$ kg/s, (b) $\dot{m} = 0.0133$ kg/s, and (c) $\dot{m} = 0.0117$ kg/s.

scheme for water and nanofluids at diverse concentrations at three mass flow rates is shown in Figure 4(a)–4(c). Higher thermal efficiency achieved was 71.02% at greater discharge of Al_2O_3 0.2% nanofluid owing to its relatively higher heat elimination rate than other cooling fluids. Similar observations have been reported earlier Kim et al. [62], Salari et al. [63], and Said et al. [64].

Both experiment and CFD modeling were used to calculate the surface T of the SPV/T system. It was found that the relationship between SPV/T surface T and efficacy and thermal efficacy is inverse. In other words, system thermal efficacy declined as SPV/T surface T rose [45]. The cooling effect of water was recorded as lower than that of the other two nanofluids, as shown in Figure 5(a)–5(c).

For a mass flow rate of 0.0117 kg/s, the variation between the observed operating fluid inlet T and collector outlet T was 11.1, 15.8, and 17.8°C for water, Al_2O_3 0.1%, and Al_2O_3 0.2% nanofluids. The energy efficiency of the collector was intrinsically linked to this T differential [46–51, 53]. For the Al_2O_3 0.2% nanofluid, the average T differential here between collector input and exit was the largest, and for water, it was the least. Furthermore, due to the closed systemic circulation used during the working fluid, the collector's working fluid inlet T was increased somewhat throughout the studies [52, 54–56].

The quantity of heat absorbed by the BF from the PV study was determined by the T of the solar cells; therefore, variations in solar cell T and water outlet T were directly

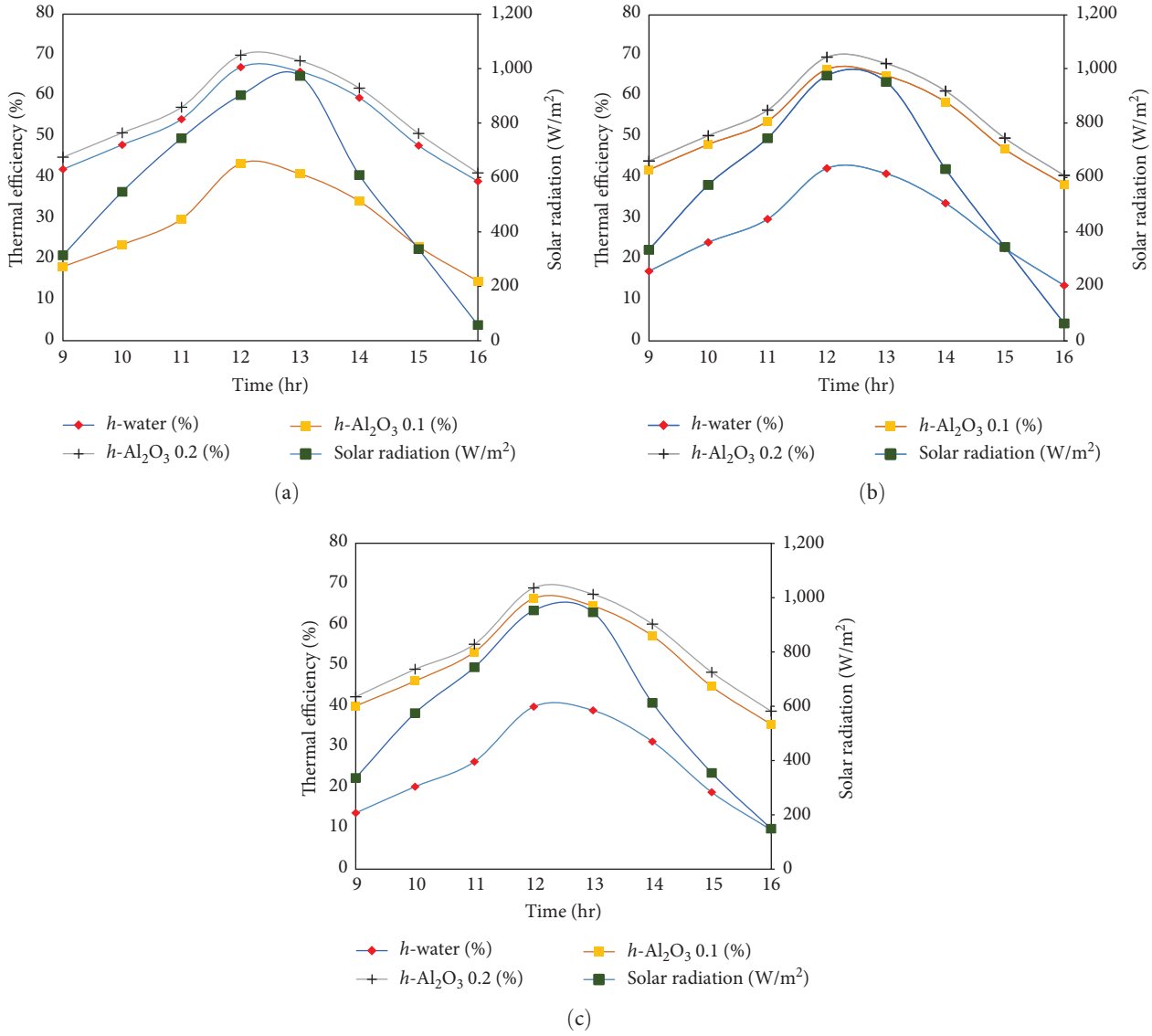

FIGURE 4: Thermal energy efficiency at the mass flow rate of (a) $\dot{m}_1 = 0.015$ kg/s, (b) $\dot{m}_2 = 0.0133$ kg/s, and (c) $\dot{m}_3 = 0.0117$ kg/s.

comparable. When combined with water and evenly dispersed by sonication, the studied Al_2O_3 nanoparticles exhibit heat transmission properties [57–61, 65]. Working fluids absorbed the least amount of heat at larger mass flow rate, due to reduced working fluid outlet T_s and the highest heat effectiveness [5].

The correlation between the T drop measured in the experiment and CFD analysis is shown in Figure 6 for all three mass flow rates. A reasonable agreement between the two approaches was found. The difference in the value is due to the discretization and round-off error, which is inherently present in CFD and cannot be made zero.

The T profile of different fluids when they flow through the serpentine heat exchanger is shown in Figure 7 for diverse mass flow rate. Obviously, the water could not carry the heat produced in the SPV/T system as per Figure 7(a) [66–69]. However, Al_2O_3 0.2% based nanofluid carried away relatively higher heat from the system [70–72].

6. Conclusion

An exergetic and energy efficacy study was accomplished for the liquid cooling enhancement of serpentine heat exchanger of 150 W solar PV thermal collectors through experimentation and numerical analysis. The liquid cooling enhancement under the test showed an increase in the rate at which heat was removed from the SPV/T system. The findings from this investigation lead to the following conclusions:

(1) Al_2O_3 0.2% resulted in an increase in exergy efficacy of 20%–36%. This is the SPV/T system's highest energy efficacy. It is clear that employing a serpentine

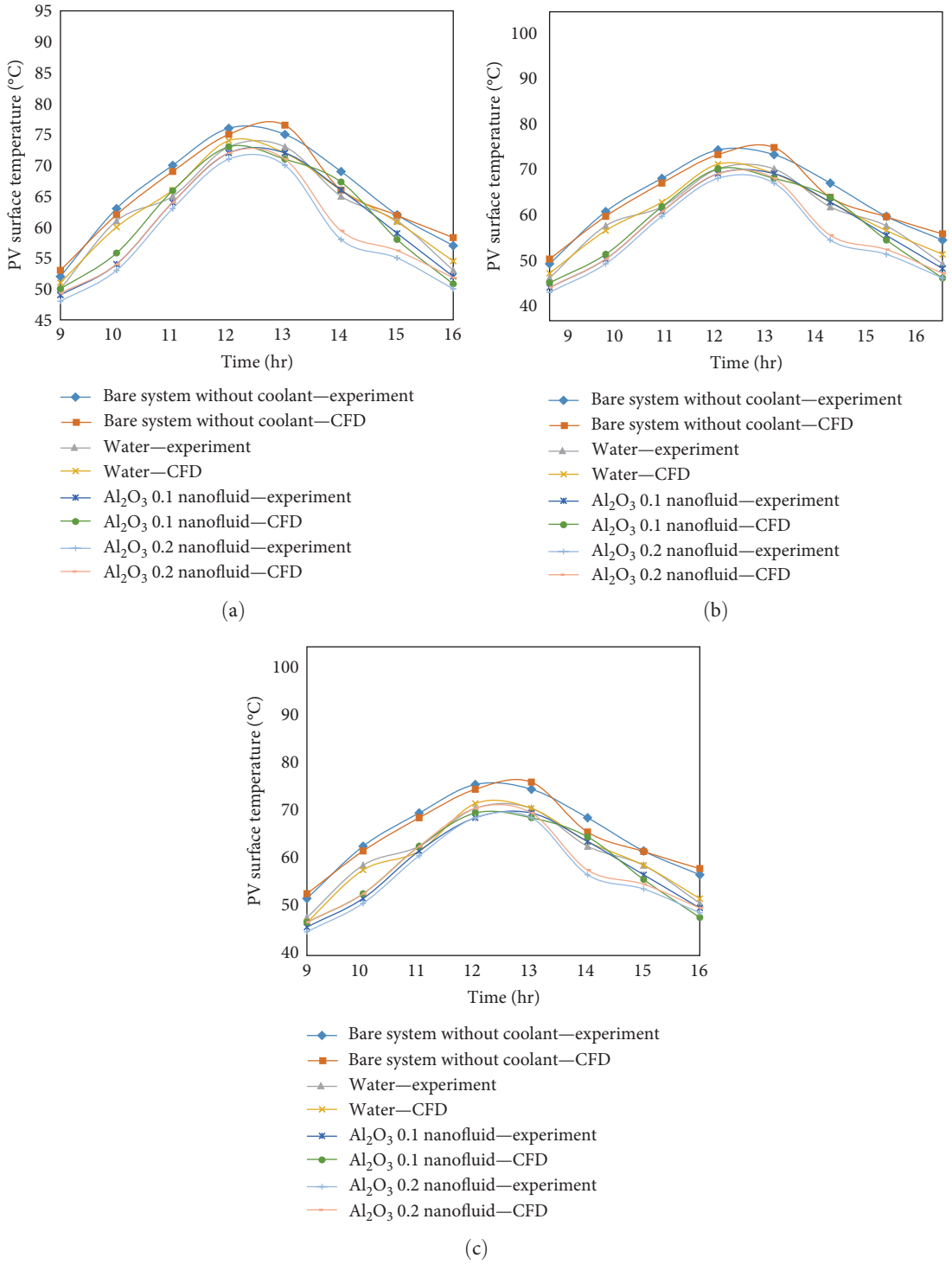

Figure 5: Photovoltaic surface temperature for mass flow rate at 0.0117 kg/s.

tube heat exchanger and a nanofluid with an Al_2O_3 0.2% base improves energy efficiency. The exergy performance was increased from 20% to 36% while using Al_2O_3 0.2%. This is the maximum exergy efficiency achieved in this SPV/T system. It can be concluded that Al_2O_3 0.2% based nanofluid increases the exergy efficiency while using a serpentine tube heat exchanger.

(2) The thermal energy performance increased by 20% using a nanofluid-based serpentine heat exchanger. Thermal efficacy is enlarged by the mass flow rate and nanoparticle concentrations. This efficacy was

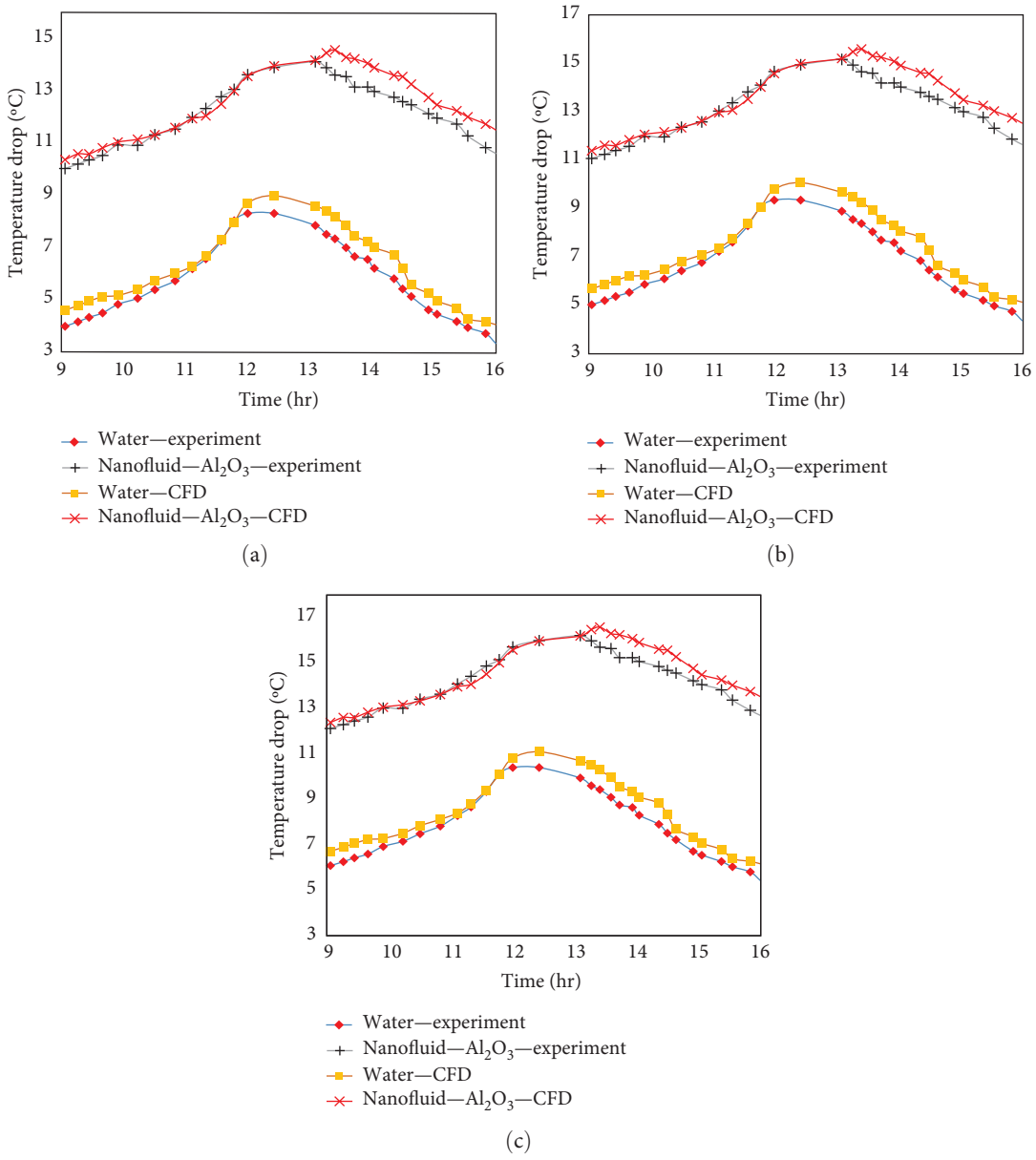

Figure 6: Temperature drop with time for different mass flow rates. (a) Mass flow rate: 0.015 kg/s, (b) mass flow rate: 0.0133 kg/s, and (c) mass flow rate: 0.0117 kg/s.

also predisposed by the intensity of solar radiation and thermophysical characteristics of the working liquids.

(3) The CFD model is found to better match test results and can be useful in upcoming parametric investigations.

(4) To boost cooling impacts and, hence, efficacy, future work might be expanded to concentrate on a more optimal serpentine copper tube heat exchanger design. Additionally, the authors can further improve the design and tube layout with various nanofluid concentrations using various CFD models.

(5) Given that it significantly reduces energy use, this setup may be applied to green and intelligent cities.

Data Availability

The data used to support the findings of this study are available from the corresponding author upon request.

Conflicts of Interest

The authors declare that they have no conflicts of interest.

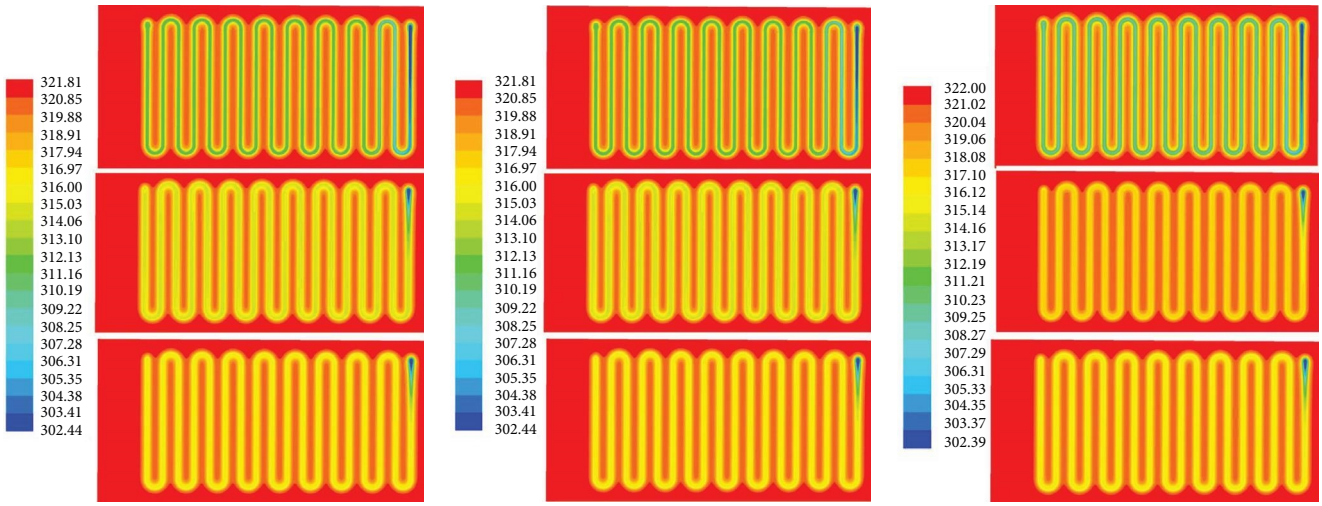

Figure 7: Temperature profile of different fluids through the serpentine heat exchanger is shown for different mass flow rate.

Acknowledgments

The authors extend their appreciation to the Deanship of Scientific Research at King Khalid University, Saudi Arabia, for funding this work through large groups under grant no. RGP 2/32/43.

References

[1] P. Dwivedi, K. Sudhakar, A. Soni, E. Solomin, and I. Kirpichnikova, "Advanced cooling techniques of P.V. modules: a state of art," *Case Studies in Thermal Engineering*, vol. 21, Article ID 100674, 2020.

[2] A. Shahsavar, A. H. A. Alwaeli, N. Azimi et al., "Exergy studies in water-based and nanofluid-based photovoltaic/thermal collectors: status and prospects," *Renewable and Sustainable Energy Reviews*, vol. 168, Article ID 112740, 2022.

[3] F. Hossain, M. R. Karim, and A. A. Bhuiyan, "A review on recent advancements of the usage of nano fluid in hybrid photovoltaic/thermal (PV/T) solar systems," *Renewable Energy*, vol. 188, pp. 114–131, 2022.

[4] B. Lalović, Z. Kiss, and H. Weakliem, "A hybrid amorphous silicon photovoltaic and thermal solar collector," *Solar Cells*, vol. 19, no. 2, pp. 131–138, 1986.

[5] A. A. Alzaabi, N. K. Badawiyeh, H. O. Hantoush, and A. K. Hamid, "Electrical/thermal performance of hybrid PV/T system in Sharjah, UAE," *International Journal of Smart Grid and Clean Energy*, vol. 3, no. 4, pp. 385–389, 2014.

[6] K. Yu, C. Park, S. Kim, H. Song, and H. Jeong, "CFD analysis of nanofluid forced convection heat transport in laminar flow through a compact pipe," *Journal of Physics: Conference Series*, vol. 885, Article ID 012021, 2017.

[7] A. Azari, M. Kalbasi, and M. Rahimi, "CFD and experimental investigation on the heat transfer characteristics of alumina nanofluids under the laminar flow regime," *Brazilian Journal of Chemical Engineering*, vol. 31, no. 2, pp. 469–481, 2014.

[8] M. Gupta and R. B. Prasad, "Potential use of nanofluids in solar collectors: a review," *SAMRIDDHI: A Journal of Physical Sciences, Engineering and Technology*, vol. 12, no. 1, pp. 32–36, 2020.

[9] J. A. Ranga Babu, K. Kiran Kumar, and S. Srinivasa Rao, "Thermodynamic analysis of hybrid nanofluid based solar flat plate collector," *World Journal of Engineering*, vol. 15, no. 1, pp. 27–39, 2018.

[10] E. Bellos, Z. Said, and C. Tzivanidis, "The use of nanofluids in solar concentrating technologies: a comprehensive review," *Journal of Cleaner Production*, vol. 196, pp. 84–99, 2018.

[11] T. Rasheed, T. Hussain, M. T. Anwar et al., "Hybrid nanofluids as renewable and sustainable colloidal suspensions for potential photovoltaic/thermal and solar energy applications," *Frontiers in Chemistry*, vol. 9, Article ID 737033, 2021.

[12] I. A. Qeays, S. M. Yahya, M. Saad Bin Arif, and A. Jamil, "Nanofluids application in hybrid photovoltaic thermal system for performance enhancement: a review," *AIMS Energy*, vol. 8, no. 3, pp. 365–393, 2020.

[13] S. M. Bambrook and A. B. Sproul, "Maximising the energy output of a PVT air system," *Solar Energy*, vol. 86, no. 6, pp. 1857–1871, 2012.

[14] K. Y. Leong, H. C. Ong, N. H. Amer, M. J. Norazrina, M. S. Risby, and K. Z. Ku Ahmad, "An overview on current application of nanofluids in solar thermal collector and its challenges," *Renewable and Sustainable Energy Reviews*, vol. 53, pp. 1092–1105, 2016.

[15] I. Wole-Osho, E. C. Okonkwo, S. Abbasoglu, and D. Kavaz, "Nanofluids in solar thermal collectors: review and limitations," *International Journal of Thermophysics*, vol. 41, Article ID 157, 2020.

[16] K. Ajay and L. Kundan, "Combined experimental and CFD investigation of the parabolic shaped solar collector utilizing nanofluid (CuO-H_2O and SiO_2-H_2O) as a working fluid," *Journal of Engineering*, vol. 2016, Article ID 5729576, 11 pages, 2016.

[17] A. J. Moghadam, M. Farzane-Gord, M. Sajadi, and M. Hoseyn-Zadeh, "Effects of CuO/water nanofluid on the efficiency of a flat-plate solar collector," *Experimental Thermal and Fluid Science*, vol. 58, pp. 9–14, 2014.

[18] E. Ekramian, S. G. Etemad, and M. Haghshenasfard, "Numerical investigations of heat transfer performance of nanofluids

in a flat plate solar collector," *International Journal of Theoretical and Applied Nanotechnology*, vol. 2, pp. 30–39, 2014.

[19] M. Shafiey Dehaj and M. Zamani Mohiabadi, "Experimental study of water-based CuO nanofluid flow in heat pipe solar collector," *Journal of Thermal Analysis and Calorimetry*, vol. 137, pp. 2061–2072, 2019.

[20] O. Mahian, A. Kianifar, S. Z. Heris, and S. Wongwises, "First and second laws analysis of a minichannel-based solar collector using boehmite alumina nanofluids: effects of nanoparticle shape and tube materials," *International Journal of Heat and Mass Transfer*, vol. 78, pp. 1166–1176, 2014.

[21] M. S. Hossain, A. K. Pandey, M. A. Tunio, J. Selvaraj, K. E. Hoque, and N. A. Rahim, "Thermal and economic analysis of low-cost modified flat-plate solar water heater with parallel two-side serpentine flow," *Journal of Thermal Analysis and Calorimetry*, vol. 123, pp. 793–806, 2016.

[22] D. B. Singh, J. K. Yadav, V. K. Dwivedi, S. Kumar, G. N. Tiwari, and I. M. Al-Helal, "Experimental studies of active solar still integrated with two hybrid PVT collectors," *Solar Energy*, vol. 130, pp. 207–223, 2016.

[23] M. Li, D. Zhong, T. Ma, A. Kazemian, and W. Gu, "Photovoltaic thermal module and solar thermal collector connected in series: energy and exergy analysis," *Energy Conversion and Management*, vol. 206, Article ID 112479, 2020.

[24] S. K. Verma, A. K. Tiwari, and D. S. Chauhan, "Experimental evaluation of flat plate solar collector using nanofluids," *Energy Conversion and Management*, vol. 134, pp. 103–115, 2017.

[25] I. Wole-Osho, E. C. Okonkwo, D. Kavaz, and S. Abbasoglu, "An experimental investigation into the effect of particle mixture ratio on specific heat capacity and dynamic viscosity of Al_2O_3-ZnO hybrid nanofluids," *Powder Technology*, vol. 363, pp. 699–716, 2020.

[26] A. Salari, A. Kazemian, T. Ma, A. Hakkaki-Fard, and J. Peng, "Nanofluid based photovoltaic thermal systems integrated with phase change materials: numerical simulation and thermodynamic analysis," *Energy Conversion and Management*, vol. 205, Article ID 112384, 2020.

[27] T. Ma, H. Yang, and L. Lu, "Development of a model to simulate the performance characteristics of crystalline silicon photovoltaic modules/strings/arrays," *Solar Energy*, vol. 100, pp. 31–41, 2014.

[28] T. Ma, M. Li, and A. Kazemian, "Photovoltaic thermal module and solar thermal collector connected in series to produce electricity and high-grade heat simultaneously," *Applied Energy*, vol. 261, Article ID 114380, 2020.

[29] D. Kong, Y. Wang, M. Li, and J. Liang, "Experimental investigation of a novel hybrid drying system powered by a solar photovoltaic/thermal air collector and wind turbine," *Renewable Energy*, vol. 194, pp. 705–718, 2022.

[30] S. M. Parsa, A. Yazdani, H. Aberoumand et al., "A critical analysis on the energy and exergy performance of photovoltaic/thermal (PV/T) system: the role of nanofluids stability and synthesizing method," *Sustainable Energy Technologies and Assessments*, vol. 51, Article ID 101887, 2022.

[31] A. Chauhan, V. V. Tyagi, and S. Anand, "Minimum entropy generation and its validation against Hottel Whillier model for PV/T and FPC collectors," *Solar Energy*, vol. 188, pp. 143–157, 2019.

[32] P. Ooshaksaraei, K. Sopian, R. Zulkifli, S. H. Zaidi, and R. Sirwan, "Performance of single pass photovoltaic thermal solar collector with bifacial solar cells," *International Review of Mechanical Engineering*, vol. 7, no. 2, pp. 358–363, 2013.

[33] S. Rashidi, L. Yang, A. Khoosh-Ahang, D. Jing, and O. Mahian, "Entropy generation analysis of different solar thermal systems," *Environmental Science and Pollution Research*, vol. 27, no. 17, pp. 20699–20724, 2020.

[34] S. Jakhar, M. K. Paliwal, and N. Purohit, "Assessment of alumina/water nanofluid in a glazed tube and sheet photovoltaic/thermal system with geothermal cooling," *Journal of Thermal Analysis and Calorimetry*, vol. 147, no. 5, pp. 3901–3918, 2022.

[35] S. Jakhar, M. K. Paliwal, and A. Kumar, "Modelling and simulation of photovoltaic thermal cooling system using different types of nanofluids," in *Advances in Air Conditioning and Refrigeration*, M. Ramgopal, S. K. Rout, and S. K. Sarangi, Eds., pp. 1–11, Springer, Singapore, 2021.

[36] S. Jakhar, M. S. Soni, and N. Gakkhar, "Performance analysis of photovoltaic panels with earth water heat exchanger cooling," *MATEC Web of Conferences*, vol. 55, Article ID 02003, 2016.

[37] F. Yazdanifard, M. Ameri, and E. Ebrahimnia-Bajestan, "Performance of nanofluid-based photovoltaic/thermal systems: a review," *Renewable and Sustainable Energy Reviews*, vol. 76, pp. 323–352, 2017.

[38] M. Sardarabadi and M. Passandideh-Fard, "Experimental and numerical study of metal-oxides/water nanofluids as coolant in photovoltaic thermal systems (PVT)," *Solar Energy Materials and Solar Cells*, vol. 157, pp. 533–542, 2016.

[39] M. Moradgholi, S. Mostafa Nowee, and A. Farzaneh, "Experimental study of using Al_2O_3/methanol nanofluid in a two phase closed thermosyphon (TPCT) array as a novel photovoltaic/thermal system," *Solar Energy*, vol. 164, pp. 243–250, 2018.

[40] N. Purohit, S. Jakhar, P. Gullo, and M. S. Dasgupta, "Heat transfer and entropy generation analysis of alumina/water nanofluid in a flat plate PV/T collector under equal pumping power comparison criterion," *Renewable Energy*, vol. 120, pp. 14–22, 2018.

[41] P. Jidhesh, T. V. Arjunan, and N. Gunasekar, "Thermal modeling and experimental validation of semitransparent photovoltaic-thermal hybrid collector using CuO nanofluid," *Journal of Cleaner Production*, vol. 316, Article ID 128360, 2021.

[42] A. Shahsavar, P. Jha, and I. B. Askari, "Experimental study of a nanofluid-based photovoltaic/thermal collector equipped with a grooved helical microchannel heat sink," *Applied Thermal Engineering*, vol. 217, Article ID 119281, 2022.

[43] A. Shahsavar, P. Jha, M. Arici, and G. Kefayati, "A comparative experimental investigation of energetic and exergetic performances of water/magnetite nanofluid-based photovoltaic/thermal system equipped with finned and unfinned collectors," *Energy*, vol. 220, Article ID 119714, 2021.

[44] E. K. Akpinar and F. Koçyiğit, "Energy and exergy analysis of a new flat-plate solar air heater having different obstacles on absorber plates," *Applied Energy*, vol. 87, no. 11, pp. 3438–3450, 2010.

[45] N. Gakkhar, M. K. Soni, and S. Jakhar, "Experimental investigation of exergy performance of a water cooled hybrid photovoltaic thermal collector," *International Journal of Exergy*, vol. 31, no. 4, pp. 330–351, 2020.

[46] A. Afzal, S. A. Khan, M. D. Islam, R. D. Jilte, A. Khan, and M. E. M. Soudagar, "Investigation and back-propagation modeling of base pressure at sonic and supersonic mach numbers," *Physics of Fluids*, vol. 32, no. 9, Article ID 096109, 2020.

[47] O. D. Samuel, M. O. Okwu, O. J. Oyejide, E. Taghinezhad, A. Afzal, and M. Kaveh, "Optimizing biodiesel production

from abundant waste oils through empirical method and grey wolf optimizer," *Fuel*, vol. 281, Article ID 118701, 2020.

[48] A. Afzal, C. A. Saleel, I. A. Badruddin et al., "Human thermal comfort in passenger vehicles using an organic phase change material–an experimental investigation, neural network modelling, and optimization," *Building and Environment*, vol. 180, Article ID 107012, 2020.

[49] A. Afzal, S. Alshahrani, A. Alrobaian, A. Buradi, and S. A. Khan, "Power plant energy predictions based on thermal factors using ridge and support vector regressor algorithms," *Energies*, vol. 14, no. 21, Article ID 7254, 2021.

[50] A. Afzal, "Optimization of thermal management in modern electric vehicle battery cells employing genetic algorithm," *ASME Journal of Heat and Mass Transfer*, vol. 143, no. 11, Article ID 112902, 2021.

[51] A. Afzal, K. M. Yashawantha, N. Aslfattahi, R. Saidur, R. K. Abdul Razak, and R. Subbiah, "Back propagation modeling of shear stress and viscosity of aqueous Ionic-MXene nanofluids," *Journal of Thermal Analysis and Calorimetry*, vol. 145, pp. 2129–2149, 2021.

[52] I. Mokashi, A. Afzal, S. A. Khan et al., "Nusselt number analysis from a battery pack cooled by different fluids and multiple back-propagation modelling using feed-forward networks," *International Journal of Thermal Sciences*, vol. 161, Article ID 106738, 2021.

[53] P. V. Elumalai, R. Krishna Moorthy, M. Parthasarathy et al., "Artificial neural networks model for predicting the behavior of different injection pressure characteristics powered by blend of biofuel-nano emulsion," *Energy Science & Engineering*, vol. 10, no. 7, pp. 2367–2396, 2022.

[54] I. Veza, A. Afzal, M. A. Mujtaba et al., "Review of artificial neural networks for gasoline, diesel and homogeneous charge compression ignition engine," *Alexandria Engineering Journal*, vol. 61, no. 11, pp. 8363–8391, 2022.

[55] H. Bakır, Ü. Ağbulut, A. E. Gürel et al., "Forecasting of future greenhouse gas emission trajectory for india using energy and economic indexes with various metaheuristic algorithms," *Journal of Cleaner Production*, vol. 360, Article ID 131946, 2022.

[56] P. Sharma, Z. Said, A. Kumar et al., "Recent advances in machine learning research for nanofluid-based heat transfer in renewable energy system," *Energy & Fuels*, vol. 36, no. 13, pp. 6626–6658, 2022.

[57] J. Sharma, S. Soni, P. Paliwal et al., "A novel long term solar photovoltaic power forecasting approach using LSTM with nadam optimizer: a case study of India," *Energy Science & Engineering*, vol. 10, no. 8, pp. 2909–2929, 2022.

[58] O. Ziaee, N. Zolfaghari, M. Baghani, M. Baniassadi, and K. Wang, "A modified cellular automaton model for simulating ion dynamics in a Li-ion battery electrode," *Energy Equipment and Systems*, vol. 10, no. 1, pp. 41–49, 2022.

[59] M. S. Taslimi, S. M. Dastjerdi, S. B. Mousavi, P. Ahmadi, and M. Ashjaee, "Assessment and multi-objective optimization of an off-grid solar based energy system for a Conex," *Energy Equipment and Systems*, vol. 9, no. 2, pp. 127–143, 2021.

[60] M. Sharifi, M. Amidpour, and S. Mollaei, "Investigating carbon emission abatement long-term plan with the aim of energy system modeling; case study of Iran," *Energy Equipment and Systems*, vol. 6, no. 4, pp. 337–349, 2018.

[61] S. Zare, M. Ayati, M. R. H. Yazdi, and A. Kabir Anaraki, "Convolutional neural networks for wind turbine gearbox health monitoring," *Energy Equipment and Systems*, vol. 10, no. 1, pp. 73–82, 2022.

[62] J.-H. Kim, J.-G. Ahn, and J.-T. Kim, "Demonstration of the performance of an air-type photovoltaic thermal (PVT) system coupled with a heat-recovery ventilator," *Energies*, vol. 9, no. 9, Article ID 728, 2016.

[63] A. Salari, A. Taheri, A. Farzanehnia, M. Passandideh-Fard, and M. Sardarabadi, "An updated review of the performance of nanofluid-based photovoltaic thermal systems from energy, exergy, economic, and environmental (4E) approaches," *Journal of Cleaner Production*, vol. 282, Article ID 124318, 2021.

[64] Z. Said, S. Arora, and E. Bellos, "A review on performance and environmental effects of conventional and nanofluid-based thermal photovoltaics," *Renewable and Sustainable Energy Reviews*, vol. 94, pp. 302–316, 2018.

[65] S. Sabzi, M. Asadi, and H. Moghbelli, "Review, analysis and simulation of different structures for hybrid electrical energy storages," *Energy Equipment and Systems*, vol. 5, no. 2, pp. 115–129, 2017.

[66] A. Afzal, A. D. M. Samee, R. K. Abdul Razak, and M. K. Ramis, "Effect of spacing on thermal performance characteristics of Li-ion battery cells," *Journal of Thermal Analysis and Calorimetry*, vol. 135, pp. 1797–1811, 2019.

[67] I. Mokashi, S. A. Khan, N. A. Abdullah, M. H. Bin Azami, and A. Afzal, "Maximum temperature analysis in a Li-ion battery pack cooled by different fluids," *Journal of Thermal Analysis and Calorimetry*, vol. 141, pp. 2555–2571, 2020.

[68] A. S. C., A. Afzal, I. A. Badruddin et al., "Numerical investigation on pressure-driven electro osmatic flow and mixing in a constricted micro channel by triangular obstacle," *International Journal of Numerical Methods for Heat & Fluid Flow*, vol. 31, no. 3, pp. 982–1013, 2021.

[69] L. Samylingam, N. Aslfattahi, R. Saidur et al., "Thermal and energy performance improvement of hybrid PV/T system by using olein palm oil with MXene as a new class of heat transfer fluid," *Solar Energy Materials and Solar Cells*, vol. 218, Article ID 110754, 2020.

[70] A. Afzal, A. D. M. Samee, R. K. A. Razak, and M. K. Ramis, "Steady and transient state analyses on conjugate laminar forced convection heat transfer," *Archives of Computational Methods in Engineering*, vol. 27, pp. 135–170, 2020.

[71] B. Benoudina, M. E. H. Attia, Z. Driss, A. Afzal, A. M. Manokar, and R. Sathyamurthy, "Enhancing the solar still output using micro/nano-particles of aluminum oxide at different concentrations: an experimental study, energy, exergy and economic analysis," *Sustainable Materials and Technologies*, vol. 29, Article ID e00291, 2021.

[72] A. R. Prasad, M. E. H. Attia, W. Al-Kouz, A. Afzal, M. M. Athikesavan, and R. Sathyamurthy, "Energy and exergy efficiency analysis of solar still incorporated with copper plate and phosphate pellets as energy storage material," *Environmental Science and Pollution Research*, vol. 28, pp. 48628–48636, 2021.